remote sensing

MDPI

Technical Note

Validation of Two Operative Google Earth Engine Applications to Generate 10 m Land Surface Temperature Maps at Daily to Weekly Temporal Resolutions

Vicente Garcia-Santos [1,*], Alejandro Buil [2], Juan Manuel Sánchez [3], César Coll [1], Raquel Niclòs [1], Jesús Puchades [1], Martí Perelló [1], Lluís Pérez-Planells [1,4], Joan Miquel Galve [3] and Enric Valor [1]

[1] Department of Earth Physics and Thermodynamics, Faculty of Physics, University of Valencia, 46100 Valencia, Spain; cesar.coll@uv.es (C.C.); raquel.niclos@uv.es (R.N.); jesus.puchades@uv.es (J.P.); martin.perello@uv.es (M.P.); lluis.perez@uv.es (L.P.-P.); enric.valor@uv.es (E.V.)
[2] Meteoclim, Calle Sophie Germain, Edificio Lleret, Planta Baja Derecha Parc Bit, 07121 Palma, Spain; alejandro.buil@wdna.com
[3] Department of Physics, University of Castilla-La Mancha, 02071 Albacete, Spain; juanmanuel.sanchez@uclm.es (J.M.S.); joanmiquel.galve@uclm.es (J.M.G.)
[4] IMK-ASF, Karlsruhe Institute of Technology (KIT), 76131 Karlsruhe, Germany; lluis.perez@kit.edu
* Correspondence: vicente.garcia-santos@uv.es

Abstract

Current land surface temperature (LST) products, estimated by sensors on board satellites, show a trade-off between their spatial and temporal resolution. If the spatial resolution is high (i.e., around 100 m), the LST product is delivered every 2 weeks, and for those LST products estimated daily, its spatial resolution is 1 km. Current spatial and temporal resolutions are not adequate for disciplines such as high-precision agriculture, urban decision making, and planning how to mitigate the overheating of cities, for which LST maps at 50–100 m resolution every few days are desirable. This situation has led to the development of disaggregation techniques in order to enhance the spatial resolution of daily LST products. Unfortunately, disaggregation techniques are usually complex since they rely on a number of external inputs and computer resources and are difficult to apply in practice. To our knowledge, there are only two operative downscaled 10 m LST products available to the end user, which are implemented in the Google Earth Engine (GEE) tool. They are the Daily Ten-ST-GEE and LST-downscaling-GEE systems. This study provides a critical benchmark by performing the first direct intercomparison and rigorous in situ validation of these two operative GEE systems. The validation, conducted with reference temperature data from dedicated field campaigns over contrasting agricultural sites in Spain, showed a good correlation of both methods with a R^2 of 0.74 for Daily Ten-ST-GEE and 0.94 for LST-downscaling-GEE, but the poor results of the first method in a highly heterogeneous site (RMSE of 5.8 K) make the second method the most suitable (RMSE of 3.6 K) for obtaining high-spatiotemporal-resolution LST maps.

Keywords: land surface temperature (LST); downscaling techniques; Google Earth Engine (GEE); temperature-based (T-b) validation

Academic Editors: Hamdi A. Zurqani and Christopher Post

Received: 16 May 2025
Revised: 7 July 2025
Accepted: 10 July 2025
Published: 10 July 2025

Citation: Garcia-Santos, V.; Buil, A.; Sánchez, J.M.; Coll, C.; Niclòs, R.; Puchades, J.; Perelló, M.; Pérez-Planells, L.; Galve, J.M.; Valor, E. Validation of Two Operative Google Earth Engine Applications to Generate 10 m Land Surface Temperature Maps at Daily to Weekly Temporal Resolutions. *Remote Sens.* **2025**, *17*, 2387. https://doi.org/10.3390/rs17142387

1. Introduction

The European Space Agency (ESA) Climate Change Initiative (CCI) Programme and the Global Climate Observing System (GCOS) stated land surface temperature (LST) as an essential climate variable (ECV). LST is required in the monitoring of the Earth climate

system [1], being of key importance in several environmental disciplines, such as climatology, hydrology or meteorology [2–5]. A significant challenge is the increase in fresh water demand for agriculture purposes around the world, requiring the need for an efficient management system for such a valuable resource [6]. In this matter, LST captured by remote sensing techniques became essential in the monitoring of water needs or irrigation scheduling [7,8].

In the last fifty years, mapping the LST over extensive areas, from continental to global scales, has become possible due to thermal infrared (TIR) sensors on board orbiting satellites [9].

However, thermal infrared (TIR) sensors face a fundamental trade-off between their spatial and temporal resolution due to physical and technical constraints [10]. On the one hand, sensors like MODIS and AVHRR provide daily data, but at a coarse spatial resolution of 1000 m. On the other hand, sensors such as the Landsat series and ASTER offer high spatial resolution (<100 m), but their long revisit time of approximately two weeks limits their use for continuous monitoring. This dilemma is significant, as high spatial resolution is necessary to minimize the impact of mixed pixels in urban studies [11,12], while a frequent revisit period is key to detect and monitor rapid surface changes in crop-growth studies [13].

High spatiotemporal requirements are expected to be met by the end of 2030, with the launch of three different missions (TRISHNA [14], LSTM [15] and SBG [16]), whose synergy will allow the daily monitoring of the LST at high spatial resolution (<60 m). To bridge this gap, a variety of LST downscaling techniques have been developed [17], which can be broadly classified into two main families. The most common are statistical methods, which are based on establishing an empirical relationship between LST and higher-resolution ancillary data (e.g., spectral indices like NDVI) through regression models [18–21]. A second family includes physics-based approaches, such as thermal unmixing, which aim to model the contribution of different surface components within a coarse pixel [10].

However, these methods do not materialize in an operative LST product that can be profited by end users. One of the main reasons is the typology of such downscaling methods, which requires significant computing power and resources to develop models and evaluate them. To our knowledge, only two studies [22,23] offer a computational tool to obtain operative LST maps at 10 m spatial resolution anywhere on the globe. Both studies took advantage of the advent of Google Earth Engine (GEE), whose high computing capabilities provide a viable alternative to the global-scale analysis of easily accessible satellite data. The GEE platform provides its users—from remote sensing specialists to a much wider audience—with access to a vast catalog of public satellite data and powerful, planetary-scale processing capabilities [24].

However, while the development of these GEE-based tools represents a significant step towards accessibility, their initial validation studies present specific limitations that leave a critical gap in understanding their performance for many end users. For instance, the Daily Ten-ST-GEE system [22] was originally validated against Landsat-8 LST as a reference, not against in situ ground measurements. This type of comparison, while useful, does not quantify the 'true' accuracy of the final product against ground-truth data. Similarly, the LST-downscaling-GEE tool [23] was validated in a single urban environment using near-surface air temperature data as a proxy for LST, a variable that is physically distinct and not directly comparable [25]. Furthermore, its performance in non-urban, heterogeneous landscapes such as agricultural areas remained untested. Consequently, a comprehensive and independent assessment of both tools using a consistent 'ground-truth' LST validation methodology, particularly within diverse agricultural settings, is currently lacking in the literature.

Therefore, the primary contribution of this work is not the development of a new methodology, but a threefold novelty based on rigorous, independent evaluation.

First, to our knowledge, this is the first study to conduct a direct intercomparison of the only two currently operative LST downscaling systems available on the GEE platform (Daily Ten-ST-GEE and LST-downscaling-GEE) using a consistent validation framework.

Second, we provide a robust and independent accuracy assessment against high-quality in situ LST measurements gathered during dedicated, multi-year field campaigns. This moves beyond inter-satellite comparisons and provides a crucial 'ground-truth' benchmark for these widely accessible tools.

Third, this validation is performed within relevant and contrasting agricultural contexts (a homogeneous rice paddy and a highly heterogeneous cropland area), providing specific guidance on the suitability of each GEE tool for agricultural monitoring, a domain where the LST-downscaling-GEE system had not previously been assessed.

The paper is structured as follows. Section 2 details the materials and methods, introducing the two GEE applications and describing the study sites, equipment, and in situ data acquisition procedures. Section 3 presents the validation results and includes a detailed discussion of the findings. Finally, Section 4 summarizes the main conclusions of this work.

2. Methodology

2.1. GEE Generator Applications of 10 m DLST Maps

2.1.1. Daily Ten-ST-GEE

Mhawej and Abunnasr [22] proposed a daily ten-meter LST (Daily Ten-ST-GEE) system, developed as a combination of remote sensing data and statistical analysis implemented in a fully automated and user-friendly open-source code in GEE. Daily Ten-ST-GEE is based on the fusion of the MOD09A1 Global Surface Reflectance (500 m, 8-Day), and MOD11A1 LST and Emissivity Daily Global (at 1 km spatial resolution), both MODIS products from Collection 6, and the 10 m surface reflectance Level-2A Sentinel 2-MSI. MODIS and Sentinel 2 datasets are available directly from the GEE platform. The authors considered the robust least squares (RLS) approach as the most appropriate machine learning approach for the LST downscaling purposes. They used the 1 km LST Terra-MODIS product to cover a longer data period and increase the temporal resolution to daily products.

The Daily Ten-ST-GEE system procedure to estimate the 10 m LST map follows the next steps: (1) Cloudy pixels in both MODIS and Sentinel 2 scenes were removed using cloud masks StateQA and QA60, respectively. (2) Median values of the Sentinel 2 and MODIS optical bands covering up to eight days from the MODIS LST overpass time were assessed. (3) Red (R), Green (G), Blue (B), Near InfraRed (NIR), Short-Wave InfraRed 1 (SWIR1) and Short-Wave InfraRed 2 (SWIR2) spectral bands from Sentinel 2 were linearly fitted to the corresponding MODIS bands, to adjust Sentinel 2 to MODIS values for the whole scene. (4) The statistical-based RLS approach was applied using MODIS 1 km LST as the dependent variable. In this step, independent variables (i.e., R, G, B, NIR, SWIR1, SWIR2) were upscaled, by simple average aggregation, to 5 km to meet the spatial resolution of the five-times-upscaled MODIS LST product. The RLS test ends with the generation of weighting coefficients. (5) The final step applies the weighting coefficients to generated 10 m R, G, B, NIR, SWIR1 and SWIR2 of Sentinel 2 (in step 3) and to the MODIS 1 km LST to obtain a final 10 m LST image. For more detailed information, the reader is referred to the work of [22].

2.1.2. LST-Downscaling-GEE

In [23], the authors implemented a downscaling method (LST-downscaling-GEE) in a GEE application to sharpen the LST derived from Landsat 8-TIRS, based on a multiple linear regression with the reflectance spectral bands of Sentinel 2-MSI increasing the spatial resolution of the LST. The model predicts the LST at 10 m spatial resolution, with spectral

indices derived from Sentinel 2-MSI bands as inputs. After inserting the input parameters, the user can select two almost-coincident Landsat 8 or 9 and Sentinel 2 images to generate a 10 m LST map. It is worth noting that it is not a daily map, but a five-daily or weekly LST map instead.

The main steps of the LST-downscaling-GEE system are as follows: (1) Retrievals of Normalized Difference Vegetation Index (NDVI, [26]), Normalized Difference Water Index (NDWI, [27]) and Normalized Difference Built-up Index (NDBI, [28]) from the surface reflectance R, G, NIR and SWIR1 bands from images of the Landsat 8-OLI (30 m) and Sentinel 2-MSI (10 m). (2) A single-channel algorithm [29] was applied to Landsat 8-TIRS band 10 to retrieve the LST at the rescaled 30 m spatial resolution. (3) A multiple linear regression downscaling approach was implemented, based on fitting a linear relation of NDVI, NDBI, NDWI (as independent variables) and LST (as dependent variable), all of them derived from Landsat 8-OLI/TIRS at 30 m spatial resolution. From this statistical model, an equation to predict 30 m LST is derived using the output coefficients. (4) Finally, a 10 m LST map is generated after applying the output coefficients of step 3 to the 10 m NDVI, NDBI, NDWI derived from spectral bands of Sentinel 2-MSI. Authors also included a residual coefficient (ΔLST10 m) estimated by subtracting the observed LST (directly from step 2) from the modeled LST (step 3) at 30 m resolution (ΔLST30 m), and then resampling to 10 m by convolution with a Gaussian kernel of 30 m.

To provide a comprehensive overview and clarify the key operational and methodological differences between the two Google Earth Engine (GEE) applications assessed in this study for generating high-spatiotemporal land surface temperature (LST) maps, Table 1 summarizes their main characteristics. This includes their underlying downscaling approaches, primary LST and high-resolution data sources, key algorithms, predictor variables, and the resulting spatial and temporal resolutions.

Table 1. Main characteristics of the Daily Ten-ST-GEE and LST-downscaling-GEE operative systems.

Key Characteristic	Daily Ten-ST-GEE	LST-Downscaling-GEE
General Methodology Type	Data Fusion/Statistical Approach	Disaggregation/Multiple Linear Regression
Primary LST Source (Coarse Resolution)	MODIS LST (1 km)	Landsat 8-TIRS LST (30 m)
High-Resolution Data Source	Sentinel-2 MSI (Optical bands)	Sentinel-2 MSI (Optical bands)
Key Algorithm/Model	Robust Least Squares (RLS)	Multiple Linear Regression (MLR)
Main Predictor Variables (from HR source)	Optical bands (R, G, B, NIR, SWIR1, SWIR2)	Spectral indices (NDVI, NDBI, NDWI)
Spatial Resolution of Output	10 m	10 m
Temporal Resolution of Output	Daily	5-daily or weekly
Residual Correction Applied?	Not explicitly mentioned as core to the method in [22]	Yes, with Gaussian kernel convolution
GEE Implementation	Yes, open-source and fully automated	Yes, user-friendly online application

2.2. Study Sites and Data

Two experimental sites were used to perform a validation of GEE LST maps against ground temperature (T_g) measurements: The Valencia test site and Las Tiesas site (Figure 1). The Valencia test site is a thermally homogeneous rice paddy area located on the East coast of Spain, near the city of Valencia, and used for calibration/validation studies of different satellite sensors [30–32]. The rice phenology induces land cover changes in the Valencia test site throughout the year, showing water-flooded soils in December–January and in May–June, bare soils trending from wet to dry in February–April, and a full vegetated landscape in July–September. The presence of these three distinct yet uniform land cover types (i.e., flooded soils, bare soils, and full vegetation) throughout the year, makes the Valencia test site a particularly interesting target for validation studies under different surface conditions and over long periods. A previous study analyzed the thermal homogeneity of the Valencia test site for the three land cover conditions and obtained standard deviations (SD) lower than 0.5 K, 0.4 K, 0.9 K for full vegetation cover, flooded, and bare soils, respectively, in an extension of 250 × 250 m^2 [31].

Ground measurements in the Valencia test site consisted of TIR radiances measured along transects in four different rice crops (Figure 1) using the hand-held multiband thermal radiometer, Cimel Electronique model CE-312, which has very high thermal accuracy [33,34]. Measurements were acquired in 33 different cloud-free days from 2018 to 2023. Ground reference temperatures were obtained after correcting TIR radiance measurements from emissivity effects, including the surface reflection of downwelling sky radiance. Emissivity was measured for different land covers with the TES method for bare soils [35] and with the Box method used for full vegetation cover [36]. The sky radiance was measured using an Infragold Reflectance Target, model Labsphere IRT-94–100, (LABSPHERE, INC. 231 Shaker Street POB 70 North Sutton, NH 03260 US [37]. Uncertainties associated with T_g data were deduced from three different error sources: (a) The uncertainty of CE-312 thermal radiometers, ranging within 0.12–0.15 K, according to an international calibration campaign [33]; (b) the spatial and temporal variability in the Valencia test site, considered as the SD of all the LST measured in the different transects within five minutes of each Landsat 8 overpass; (c) and the uncertainty in the emissivity correction due to errors in sky radiance and emissivity. Finally, an average error of 0.7 K was obtained for a T_g range of 282–316 K.

The second experimental site is located in a cropland area in "Las Tiesas" agricultural station, in the southeastern part of Spain (Figure 1). It is a very flat area at 700 m a.s.l. used in international campaigns [38,39]. Las Tiesas site combines irrigated and rainfed crops of different extensions ranging from 1 ha to large fields over 50 ha. Table 2 lists the type of crop, geographic coordinates and date for the ground data available for both experimental sites in this study.

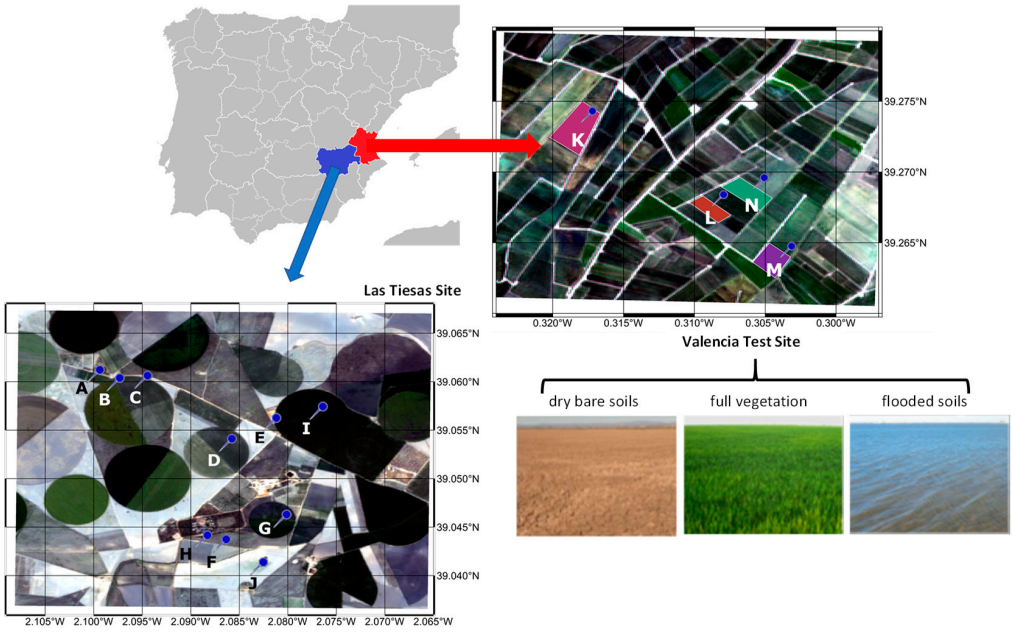

Figure 1. Location of the Valencia and Las Tiesas test sites in Spain. Pictures of different soils/vegetation covers throughout the year for the Valencia test site are included. Letters refer to the ID assigned to each plot (see Table 2).

Ground reference measurements of T_g were acquired at the Las Tiesas site with intensive field campaigns during the summer seasons of 2018–2019 for different crops (barley, vineyard, garlic, poppy, wheat, bare soils, and almond orchard; see Table 2), with the aim of encompassing a variety of different vegetation cover conditions [40]. All selected plots have an average extension greater than 10 ha (except for the vineyard with an extension of around 5 ha). T_g data were acquired along transects with several Apogee

MI-210 hand-held infrared radiometers carried at a height of 1.5–2 m above the ground surface. These radiometers measure the radiance in the 8–14 μm TIR region with a field of view of 22°. Apogee MI-210 radiometers showed an accuracy of 0.3 K after calibrations with a black body Landcal-P80 [41], performed before and after every campaign. For sparse crops (vineyard and almond orchards), T_g measurements were taken by averaging soil and canopy component temperatures to obtain representative values at a crop level. Because radiometers actually measure the TIR radiances, as in the case of the Valencia test site, they were also corrected for emissivity effects. A total of 44 measurements were acquired at different crops concurrently with the overpass of the Landsat 8 satellite on 11 different cloud-free days from 2018 to 2019. For more specific details about the field campaigns carried out at the Las Tiesas Site, the reader is referred to [19,40].

Table 2. Crop type, geographic location and date of the T_g acquisition, for each plot measured in several field campaigns in both sites. Crop IDs A–J correspond to Las Tiesas and K–N to Valencia.

Crop ID	Crop Type	Latitude (°)	Longitude (°)	Date (Year: Month/Day)
A	Vineyard	39.0598	−2.1009	2018: 6/15, 7/17, 7/24, 8/2 2019: 7/11
B	Poppy	39.0592	−2.0989	2018: 6/15, 6/22, 7/24 2019: 7/11
C	Garlic	39.0592	−2.0958	2018: 6/15, 6/22 2019: 7/11
D	Garlic Pivot	39.0529	−2.0872	2018: 6/15, 6/22
E	Bare Soil	39.0545	−2.083	2018: 6/15, 6/22, 7/17, 7/24, 8/2
F	Barley (rainfed)	39.0426	−2.0877	2018: 6/15, 6/22, 7/17, 7/24
G	Barley (irrigation)	39.045	−2.0814	2018: 6/15, 7/8, 7/17
H	Almonds	39.0429	−2.0895	2018: 6/15, 7/8, 7/17, 7/24, 8/2, 8/25, 10/5, 10/12 2019: 7/11, 8/28
I	Wheat	39.0561	−2.0774	2018: 6/22, 7/17, 7/24
J	Bare Soil	39.0402	−2.0849	2018: 6/22
K	Rice field	39.2729	−0.3185	2018: 3/27, 9/20 2021: 12/8 2022: 2/3, 2/10, 5/17, 8/21, 9/6 2023: 1/12, 1/21, 1/28
L	Rice field	39.2681	−0.3092	2018: 5/7, 6/15, 7/10, 7/17 2019: 1/16, 1/21, 1/25, 2/22, 2/26 2022: 8/5, 4/24, 5/1, 5/10, 5/26, 7/4, 7/13
M	Rice field	39.264	−0.3045	2022: 8/5, 8/14
N	Rice field	39.2689	−0.3072	2023: 4/2, 4/18, 5/13, 5/20

3. Results

It is important to note that the Daily Ten-ST-GEE and LST-downscaling-GEE systems, while both generating 10 m LST maps, rely on different original LST products as their primary input for downscaling: MODIS 1 km LST for the former and Landsat 8-TIRS 30 m LST for the latter. This fundamental difference in input sources must be considered when interpreting the comparative results presented hereafter.

3.1. Assessment of Downscaled LST Maps

Figure 2 presents LST maps for June 15, 2018, encompassing the original Landsat 8 LST at 30 m resolution (Figure 2a,d), and the downscaled 10 m LST products from both Daily Ten-ST-GEE (Figure 2b,e) and LST-downscaling-GEE systems (Figure 2c,f) for the Valencia and Las Tiesas sites, respectively. A visual assessment of Figure 2 reveals significant differences not only between the two downscaling methods, but also in how each method refines the spatial patterns observed in the original Landsat 8 LST. A minor difference in the spatial coverage between the two Valencia maps (Figure 2b,c) is also apparent, likely due to the different input data sources and their respective quality masks, with the MODIS-based Daily Ten-ST-GEE method resulting in more invalid pixels at the scene edges. Regarding the thermal patterns in Las Tiesas, the LST-downscaling-GEE map (Figure 2f) shows the expected contrast between cool, irrigated croplands and warmer surrounding soil. Conversely, the Daily Ten-ST-GEE result (Figure 2e) displays a spatially unrealistic pattern, an issue that is analyzed in detail in Section 4.2, where we attribute it to the coarse input resolution and lack of residual correction. Notably, the Daily Ten-ST-GEE method generally exhibits higher LST values and a narrower temperature range compared to the LST-downscaling-GEE system, with these discrepancies being particularly pronounced in the highly heterogeneous site of Las Tiesas (Figure 2e,f). These distinctions can be attributed to fundamental methodological differences, primarily related to their initial LST input resolution, downscaling strategies, and the handling of regression residuals.

The performance of the Daily Ten-ST-GEE system is largely due to its reliance on MODIS 1 km LST products as the coarse-resolution input for downscaling. The method applies a robust least squares (RLS) approach where MODIS data are upscaled to 5 km for model training. This substantial upscaling to 5 km for the RLS regression, particularly in heterogeneous environments like Las Tiesas, inevitably leads to an overestimation of LST. The coefficients derived from these coarser, often mixed, MODIS pixels may not accurately represent the finer-scale thermal variations, resulting in a reduction in the overall LST range. This effect is explained by [42], where it is suggested to consider LST–descriptor relationships at a native (coarse) resolution, since scale-invariant LST at finer resolutions can be troublesome in heterogeneous environments, where variations in spatial resolution can cause changes in spatial variation within a pixel area. Visually comparing the Daily Ten-ST-GEE LST (Figure 2b,e) with the original Landsat 8 LST (Figure 2a,d), the Daily Ten-ST-GEE products sometimes appear to lose some of the subtle spatial detail present in Landsat, especially in heterogeneous areas like Las Tiesas, where the boxy effect is visible when compared to the original Landsat LST. Furthermore, the Daily Ten-ST-GEE method does not explicitly include a residual correction step. This absence significantly contributes to the noticeable 'boxy effect' observed in highly varied landscapes (Figure 2e). A pixel re-scaled at 5 km from MODIS reflectance bands often fails to represent the reflectance values in a smaller, heterogeneous area, thus impacting the downscaled product. While this approach may prove more reliable in thermally homogeneous areas, where a 1×1 km^2 or 5×5 km^2 pixel is representative of similar spectral reflectance values (as seen in Figure 2b, matching the broader patterns of Figure 2a), its performance degrades considerably in a variety of agricultural landscapes like Las Tiesas.

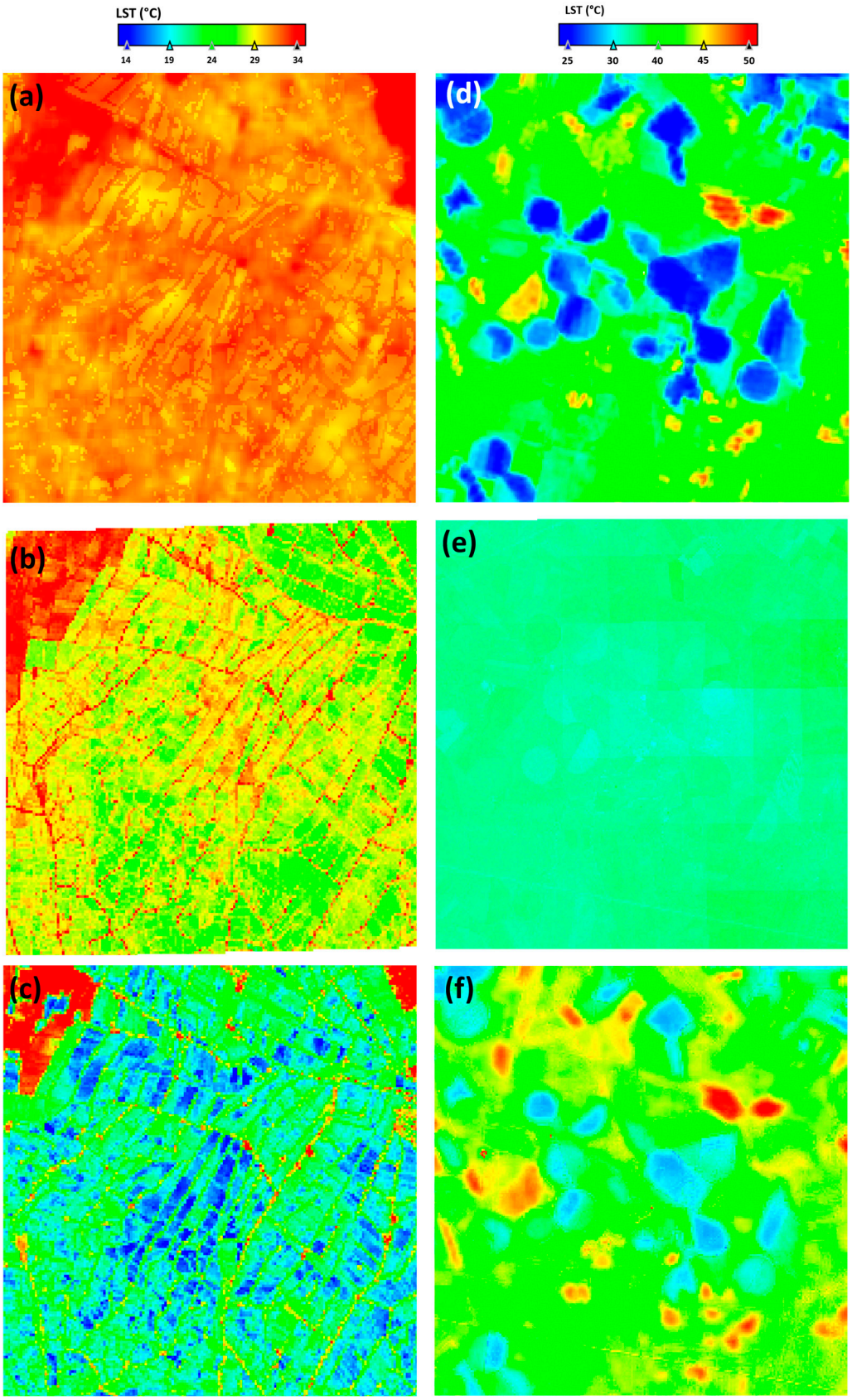

Figure 2. LST maps for 15 June 2018. Valencia test site: (**a**) Original Landsat 8 LST, (**b**) Daily Ten-ST-GEE LST, and (**c**) LST-downscaling-GEE LST. Las Tiesas test site: (**d**) Original Landsat 8 LST, (**e**) Daily Ten-ST-GEE LST, and (**f**) LST-downscaling-GEE LST.

Conversely, the LST-downscaling-GEE system generally provides a better definition of thermal elements and a more realistic LST range in heterogeneous areas (Figure 2f), showing improved discrimination between warmer and colder surfaces, and without the apparent 'boxy effect'. Comparing LST-downscaling-GEE maps (Figure 2c,f) with the original Landsat 8 LST (Figure 2a,d), it is evident that this method successfully sharpens the thermal patterns of Landsat while preserving the overall spatial distribution. This is primarily because its downscaling approach starts from Landsat 8-TIRS LST at 30 m resolution, which is inherently closer to the target 10 m resolution compared to MODIS 1 km LST. The regression performed with 30 m Landsat spectral bands, applied to 10 m Sentinel-2 bands, offers a more realistic representation of mixed zones. Additionally, this method includes a crucial residual correction coefficient, which is estimated by subtracting the observed LST from the modeled LST and applied to the disaggregated results [19,43]. This step is key for improving results and preserving thermal variability. However, a specific drawback of this method is that applying regression coefficients estimated from Landsat 8 bands to Sentinel 2 bands can lead to a narrowing of the LST range values, resulting in a smoothing of crop boundaries (Figure 2f). A more suitable procedure could involve harmonizing the spectral index values between Landsat-8 and Sentinel-2 prior to a regression application [44].

3.2. Quantitative Validation Against In Situ Measurements

To assess the accuracy of the 10 m LST maps estimated by both GEE systems, we averaged and calculated the SD for the LST values of the 10 × 10 pixel centered in the geographic coordinates of each plot in Las Tiesas site (see Table 2 in Section 2.2), and for the pixels within the area covered by each field in the Valencia test site (Figure 1). The aim was to match the spatial representativeness of the T_g measurements made in each transect. It should be noted that, in the case of the Valencia test site, just 23 dates (23 points) were possible to match with the Daily Ten-ST-GEE system in this site, since this code no longer estimated LST maps for dates in 2023 (7 points in total), and 3 more dates were also unavailable in previous years due to code execution problems. Figure 3 shows the scatterplots of 10 m LSTs against the ground-measured values for the two sites and methods. Table 3 shows the statistical metrics of the validation: correlation coefficient (R^2), mean absolute error (MAE), mean bias error (MBE), and root mean square error (RMSE) [45].

In the case of the Valencia test site, both methods show a good correlation with the ground LST data. The Daily Ten-ST-GEE method showed RMSE and MAE of 2.0 K and 1.6 K, respectively, being lower than those obtained with the LST-downscaling GEE method (4.1 K and 3.3 K, respectively). In terms of MBE, the second method showed a slightly smaller value than the first one. Therefore, the Daily Ten-ST-GEE system is more accurate than the LST-downscaling-GEE method in thermally homogeneous areas such as the Valencia test site.

However, validation results at the Las Tiesas site showed better results for the LST-downscaling-GEE method. The poor results of the Daily Ten-ST-GEE method can only be understood from the perspective that Las Tiesas is a highly heterogeneous site, and because of the scaling effect consequences [42] previously described in this section. The approach suggested by this method, i.e., synergy between MODIS (1 km) and Sentinel 2-MSI (10 m), cannot capture the high thermal variability that occurs in areas less than 500 × 500 m^2, as in the case of Las Tiesas.

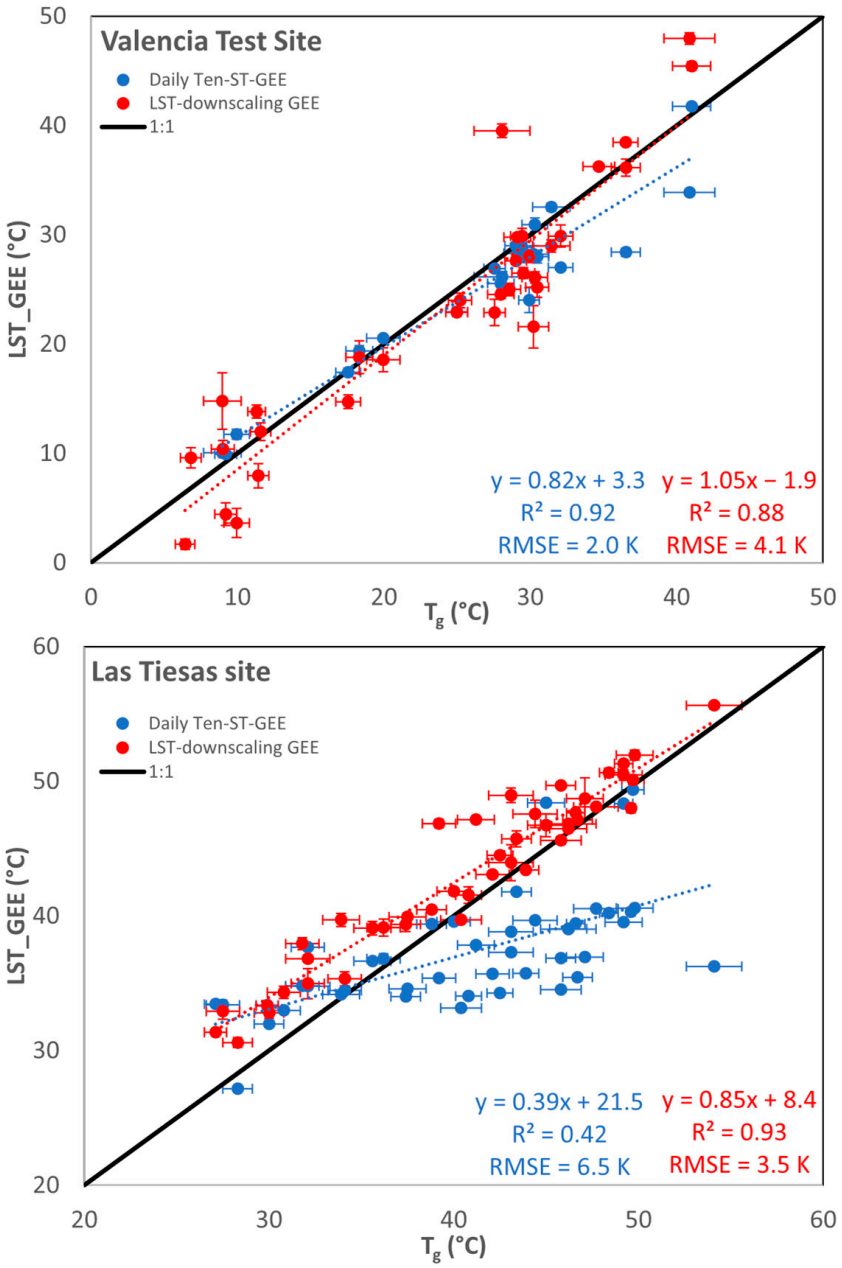

Figure 3. Scatter plots of the validation performed in both study sites when comparing LST data generated with both codes (Daily Ten-ST-GEE and LST-downscaling-GEE) with reference ground temperature data measured in several field campaigns. Blue and red dashed lines are the corresponding regressions lines for Daily Ten-ST-GEE and LST-downscaling-GEE methods, respectively.

Table 3. Statistical results (R^2, MBE, MAE and RMSE) for the ground–GEE LST comparison in both sites separately and in total.

	Daily Ten-ST-GEE			LST-Downscaling-GEE		
	Valencia	**Las Tiesas**	**Total**	**Valencia**	**Las Tiesas**	**Total**
R^2	0.92	0.42	0.74	0.88	0.93	0.94
MBE (K)	1.1	3.6	2.8	0.8	−2.3	−1.0
MAE (K)	1.6	5.3	4.5	3.3	2.5	2.8
RMSE (K)	2.0	6.5	5.8	4.1	3.1	3.6

4. Discussion

4.1. Comparison with Previous Studies

It is worth noting that the two GEE methods were validated with different types of data in their original publications. The LST-downscaling-GEE method was validated with in situ data at different spots of an urban environment (Košice, Slovakia), showing a high RMSE value (4.2 K). However, they used air temperatures in different sites around the city as reference, which are not directly comparable with LSTs [25]. The present study demonstrated that the LST-downscaling-GEE method shows better RMSE values as compared with ground LST measurements, at least in agricultural areas.

On the other hand, the Daily Ten-ST-GEE method was originally validated against Landsat-8 LST products in three agricultural and three urban sites (one Landsat-8 scene per site). The results showed an average RMSE of 1.7 K and 1.6 K at the agricultural and urban sites, respectively. The results of the validation of this method in the highly homogeneous agricultural site of the Valencia agree with those shown in the original study, but are much worse in the Las Tiesas site, where the heterogeneity of crops is a challenge for the Daily Ten-ST-GEE method. It seems that this method performs well in urban areas according to their validation results.

For purposes of accuracy comparison, it is also useful to compare our results with standard LST products from Landsat. In the Valencia test site, LSTs from Landsat 7-ETM+, Landsat 8-TIRS and Landsat 9-TIRS2 showed RMSEs of 0.8 K [46], 1.5 K [32], and 1.1 K [47], respectively, when compared with ground temperatures. In the Las Tiesas site, previous validation studies for accuracy comparison purposes showed a RMSE of 1.6 K for Landsat 7-ETM+ [48] and of 1.8 K for Landsat 8-TIRS [19]. This indicates that the accuracy of the GEE-downscaled products is still lower than that of the standard Landsat LST products.

Previous research has demonstrated the effectiveness of also combining shortwave-multispectral Sentinel-2 MSI observations with thermal-infrared Sentinel-3 SLSTR observations to derive daily, field-scale LST data. Ref. [19] explored the potential of fusing the Sentinel-2 (S2) and Sentinel-3 (S3) constellation with the focus on semi-arid agricultural areas. Maps of LST with 10–20 m spatial resolution were obtained, covering the Las Tiesas experimental site, for a set of 14 different dates in the summers of 2018–2019 and compared to ground measurements of LST as well as against LST from Landsat-8/TIRS images in a cross-validation. Differences with observed values resulted in an average RMSE < 3.0 K and a negligible systematic deviation. These authors pointed to the need for appropriate adjustment techniques of the obtained LST residuals to better capture low-temperature conditions, for instances in irrigated areas. Ref. [20] addressed this limitation by incorporating Landsat information retaining the longwave radiance emission captured by the Sentinel-3 thermal bands at its native resolution. These authors reported a reduction in RMSE of up to 1.5 K when compared to previous research.

However, the results of the two models tested here are not as good as those obtained in other dedicated field campaigns for the validation of rescaled 10 m LST maps, as is the specific case for the Las Tiesas site [18–20]. It is important to highlight that the advantages of both models are their operability and easy availability for the end user, without ignoring that both models have deficiencies that can be addressed.

4.2. Discussion on Model Performance and Variability

A closer inspection of the validation results for the Daily Ten-ST-GEE method (Figure 3) reveals another important aspect. While a systematic overestimation is observed on average (as indicated by the positive MBE in Table 3), the performance is not consistent across all acquisition dates. Several data points lie close to the 1:1 line, suggesting a significant day-to-day variability in the accuracy of the model. This daily performance variability can

likely be attributed to several dynamic factors that influence the accuracy of the input data and the assumptions of the downscaling model.

Several factors could contribute to this variability, one of which is the viewing geometry of the satellite. MODIS has a wide swath, leading to large variations in view zenith angle from day to day. Off-nadir acquisitions are more susceptible to introducing uncertainties in the initial 1 km LST product [49] that are then propagated through downscaling. Atmospheric conditions, such as the presence of sub-pixel clouds or high aerosol loads on specific days, can also impact the quality of the MODIS LST input. Furthermore, the state of the surface itself, including crop phenological stage and soil moisture content [50] following irrigation or precipitation events, alters the thermal and spectral properties of the landscape. The static relationship assumed by the downscaling model between LST and the predictor variables may not hold equally well under all these varying surface conditions. A detailed day-by-day analysis would be required to disentangle the specific impact of each of these factors, which is beyond the scope of the current study.

The LST-downscaling-GEE method [23] is a better alternative to operatively retrieve a 10 m LST map. From the combined validation results (total in Table 3), the following is shown: an overestimation in LST of 1 K with respect to the in situ values, good correlation (0.94), MAE of 2.8 K, and RMSE of 3.6 K. This is significantly lower than the RMSE of 5.8 K for the Daily Ten-ST-GEE method. The LST-downscaling-GEE system also showed a good representation of the thermal spatial variability of homogeneous and heterogeneous areas, as well as the best accuracy shown in the validation of its LST product with in situ data. It is currently, in our opinion, the best option to obtain operative high-spatiotemporal LST maps.

However, this conclusion based on accuracy must be contextualized with the different temporal resolutions of the two systems. The higher temporal frequency of the Daily Ten-ST-GEE method (daily) increases the likelihood of obtaining at least one cloud-free observation over a short period, which is a critical advantage, for instance, in time-sensitive applications like monitoring incipient water stress. This benefit, however, comes at the cost of the lower accuracy shown in this study. Conversely, the LST-downscaling-GEE method provides a more accurate LST map, but its reliance on less frequent Landsat overpasses increases the risk of long data gaps due to clouds. Therefore, the choice of the 'best' method involves a crucial trade-off, where end users must decide whether their application prioritizes the higher probability of a timely but less accurate LST map or a more accurate but less temporally reliable one.

4.3. Challenges and Future Perspectives in High-Spatiotemporal LST Generation

Despite the clear value of the operative GEE tools evaluated in this study, their performance highlights that significant challenges remain for the routine generation of reliable high spatiotemporal LST products. A key operational limitation is the frequent data loss due to cloud cover. Optical and thermal infrared sensors cannot penetrate clouds, creating substantial temporal gaps that limit the applicability of these products for continuous monitoring applications, such as daily irrigation scheduling or drought assessment. As demonstrated in this work, another key challenge is the generalizability of the downscaling algorithms. The performance of a model can be highly dependent on the spatial heterogeneity of the landscape, with methods calibrated for homogeneous areas potentially failing to capture the thermal complexity of more varied environments. Finally, the quality and characteristics of the initial input data remain a fundamental constraint, forcing a choice between the high temporal frequency of coarse-resolution sensors like MODIS and the high spatial detail of less frequent sensors like Landsat.

However, several promising avenues are emerging to address these challenges and define the future of LST monitoring. To overcome the cloud cover issue, a key perspective

is the fusion of TIR data with passive microwave observations, which can retrieve LST in all-weather conditions, but at a much coarser spatial resolution. The evolution of machine learning and deep learning models also offers significant potential. Unlike the linear statistical methods often used, these advanced algorithms (e.g., Random Forests, Convolutional Neural Networks) can better model the complex, non-linear relationships between LST and surface predictors, potentially improving accuracy in heterogeneous landscapes. Lastly, the upcoming generation of satellite missions is ready to directly mitigate the spatiotemporal trade-off. Missions such as the Copernicus Land Surface Temperature Monitoring (LSTM) or TRISHNA are designed to provide native LST data, at high resolution (tens of meters) with a high revisit frequency (every few days), which will reduce the reliance on complex downscaling LST algorithms.

5. Conclusions

This study rigorously assessed the performance of two operative Google Earth Engine (GEE) applications—Daily Ten-ST-GEE and LST-downscaling-GEE—for generating 10 m land surface temperature (LST) maps across several agricultural environments. Both models demonstrated an adequate representation of 10 m LST maps in the thermally homogeneous Valencia test site, characterized by large extensions of rice fields. However, significant differences in their performance were observed in the highly heterogeneous site of Las Tiesas, composed of different crop types. The LST-downscaling-GEE method consistently proved to be the more suitable option for such heterogeneous landscapes (RMSE of 3.6 K), providing a more realistic representation of mixed zones and a greater range of LSTs due to its reliance on Landsat 8 (30 m) LST as primary input. Conversely, the Daily Ten-ST-GEE method (RMSE of 5.8 K), using MODIS (1 km) LST data, was notably influenced by scale effects, leading to overestimation and a narrower LST range in complex agricultural areas. Both operative models show suitability for use in agricultural environments. Nevertheless, our findings indicate that the choice of GEE system should be guided by the specific heterogeneity of the crop types present in the scene, with LST-downscaling-GEE being a preference for more varied landscapes.

Beyond the direct comparison of these two GEE tools, this work provides a significant contribution to the field by establishing a crucial benchmark for the accuracy and practical utility of 'push-button', operational high-resolution LST products within the GEE environment. By demonstrating the real performance and specific limitations of these widely accessible tools against rigorous in situ ground-truth data, this study provides valuable information to assist the broad community of end user (i.e., agriculture, urban planning, and other environmental disciplines), in selecting the most appropriate tool. It underscores the critical need for independent validation of such ready-to-use systems before their application in decision-making processes, highlighting that even operative tools require careful assessment of their suitability for specific, heterogeneous environments.

Despite these contributions, our study has certain limitations. The validation was conducted in two specific agricultural regions in Spain, which, while diverse in heterogeneity, do not cover the full spectrum of global land cover or climatic conditions. Future research should focus on expanding the validation of these and similar downscaling methods to a broader range of distinct geographical and climatic regions, potentially incorporating data from established global networks where LST validation best practices are followed. Additionally, further investigations could explore the integration of advanced machine learning algorithms within these operative GEE frameworks to potentially mitigate some of the observed limitations, such as the smoothing of LST patterns or overestimation in highly heterogeneous areas.

Author Contributions: Conceptualization, V.G.-S., A.B. and J.M.S.; methodology, V.G.-S.; validation, J.P., L.P.-P., M.P. and J.M.G.; formal analysis V.G.-S. and A.B.; investigation, V.G.-S.; resources, J.M.S. and R.N.; data curation, A.B., J.M.S. and R.N.; writing—original draft preparation, V.G.-S.; writing—review and editing, J.M.S., C.C., E.V. and R.N.; visualization, V.G.-S.; supervision, C.C.; project administration, J.M.S., E.V. and R.N.; funding acquisition, J.M.S., E.V. and R.N. All authors have read and agreed to the published version of the manuscript.

Funding: This research was funded Spanish Ministry of Science and Innovation and the Spanish State Research Agency (MCIN/AEI/10.13039/501100011033) under Project PID2020-118797RBI00. This work was also funded by the Education, Culture and Sports Council (JCCM, Spain) (project SBPLY/21/180501/000070) and the Agencia Estatal de Investigación (project TED2021–130405B-I00), together with FEDER and Next Generation EU/PRTR co-financing.

Data Availability Statement: The data presented in this study are available on request from the corresponding author.

Acknowledgments: The authors used the GEE tool provided by Mhawej, M.; Abunnasr, Y. for the Daily Ten-ST-GEE application and by Onačillová, K. for the LST-downscaling-GEE application to retrieve LST maps at high spatiotemporal resolutions in the two validation sites. The authors have reviewed and edited the output and take full responsibility for the content of this publication.

Conflicts of Interest: The authors declare no conflicts of interest.

References

1. *The 2022 GCOS Implementation Plan GCOS-244 GOOS-272*; Global Climate Observing System: Geneva, Switzerland, 2022.
2. Weng, Q. Thermal Infrared Remote Sensing for Urban Climate and Environmental Studies: Methods, Applications, and Trends. *ISPRS J. Photogramm. Remote Sens.* **2009**, *64*, 335–344. [CrossRef]
3. Anderson, M.C.; Allen, R.G.; Morse, A.; Kustas, W.P. Use of Landsat Thermal Imagery in Monitoring Evapotranspiration and Managing Water Resources. *Remote Sens. Environ.* **2012**, *122*, 50–65. [CrossRef]
4. Mokhtari, A.; Noory, H.; Pourshakouri, F.; Haghighatmehr, P.; Afrasiabian, Y.; Razavi, M.; Fereydooni, F.; Sadeghi Naeni, A. Calculating Potential Evapotranspiration and Single Crop Coefficient Based on Energy Balance Equation Using Landsat 8 and Sentinel-2. *ISPRS J. Photogramm. Remote Sens.* **2019**, *154*, 231–245. [CrossRef]
5. Trigo, I.F.; Boussetta, S.; Viterbo, P.; Balsamo, G.; Beljaars, A.; Sandu, I. Comparison of Model Land Skin Temperature with Remotely Sensed Estimates and Assessment of Surface-Atmosphere Coupling. *J. Geophys. Res. Atmos.* **2015**, *120*, 12096–12111. [CrossRef]
6. The State of Food and Agriculture 2014 (SOFA). 2014. Available online: https://www.fao.org/documents/card/en?details=839a2f5e-5c1e-48b7-8370-9681c4f62906 (accessed on 7 November 2023).
7. Kalma, J.D.; McVicar, T.R.; McCabe, M.F. Estimating Land Surface Evaporation: A Review of Methods Using Remotely Sensed Surface Temperature Data. *Surv. Geophys.* **2008**, *29*, 421–469. [CrossRef]
8. Peng, J.; Nieto, H.; Neumann Andersen, M.; Kørup, K.; Larsen, R.; Morel, J.; Parsons, D.; Zhou, Z.; Manevski, K. Accurate Estimates of Land Surface Energy Fluxes and Irrigation Requirements from UAV-Based Thermal and Multispectral Sensors. *ISPRS J. Photogramm. Remote Sens.* **2023**, *198*, 238–254. [CrossRef]
9. Li, Z.L.; Tang, B.H.; Wu, H.; Ren, H.; Yan, G.; Wan, Z.; Trigo, I.F.; Sobrino, J.A. Satellite-Derived Land Surface Temperature: Current Status and Perspectives. *Remote Sens. Environ.* **2013**, *131*, 14–37. [CrossRef]
10. Wang, J.; Schmitz, O.; Lu, M.; Karssenberg, D. Thermal Unmixing Based Downscaling for Fine Resolution Diurnal Land Surface Temperature Analysis. *ISPRS J. Photogramm. Remote Sens.* **2020**, *161*, 76–89. [CrossRef]
11. Zakšek, K.; Schroedter-Homscheidt, M. Parameterization of Air Temperature in High Temporal and Spatial Resolution from a Combination of the SEVIRI and MODIS Instruments. *ISPRS J. Photogramm. Remote Sens.* **2009**, *64*, 414–421. [CrossRef]
12. Bonafoni, S.; Anniballe, R.; Gioli, B.; Toscano, P. Downscaling Landsat Land Surface Temperature over the Urban Area of Florence. *Eur. J. Remote Sens.* **2016**, *49*, 553–569. [CrossRef]
13. Olivera-Guerra, L.; Mattar, C.; Merlin, O.; Durán-Alarcón, C.; Santamaría-Artigas, A.; Fuster, R. An Operational Method for the Disaggregation of Land Surface Temperature to Estimate Actual Evapotranspiration in the Arid Region of Chile. *ISPRS J. Photogramm. Remote Sens.* **2017**, *128*, 170–181. [CrossRef]

14. Lagouarde, J.P.; Bhattacharya, B.K.; Crébassol, P.; Gamet, P.; Babu, S.S.; Boulet, G.; Briottet, X.; Buddhiraju, K.M.; Cherchali, S.; Dadou, I.; et al. The Indian-French Trishna Mission: Earth Observation in the Thermal Infrared with High Spatio-Temporal Resolution. In Proceedings of the 2018 International Geoscience and Remote Sensing Symposium (IGARSS), Valencia, Spain, 22–27 July 2018; pp. 4078–4081. [CrossRef]
15. Koetz, B.; Baschek, B.; Bastiaanssen, W.; Berger, M.; Blommaert, J.; Alamanac, A.B.; Barat, I.; Fabrizia Buongiorno, M.; D'andrimont, R.; Bello, U.D.; et al. ESA UNCLASSIFIED-For ESA Official Use Only Title Copernicus High Spatio-Temporal Resolution Land Surface Temperature Mission: Mission Requirements Document Issue Number 3 Revision Number 0. 2021. Available online: https://sentiwiki.copernicus.eu/__attachments/1678167/ESA-EOPSM-HSTR-MRD-3276%20-%20Copernicus%20High%20Spatio-Temporal%20Resolution%20Land%20Surface%20Temperature%20Mission%202021%20-%203.0.pdf?inst-v=5f22af6a-d79a-4a5b-a820-1fdb4aabe8f4 (accessed on 9 July 2025).
16. Lee, C.M.; Glenn, N.F.; Stavros, E.N.; Luvall, J.; Yuen, K.; Hain, C.; Schollaert Uz, S. Systematic Integration of Applications into the Surface Biology and Geology (SBG) Earth Mission Architecture Study. *J. Geophys. Res. Biogeosci.* **2022**, *127*, e2021JG006720. [CrossRef]
17. Li, Z.-L.; Liu, X.; Zhao, E.; Si, M.; Gao, C.; Wu, H.; Ren, H.; Duan, S.-B.; Tang, R.; Tang, B.-H.; et al. Reflections on Developments and Opportunities of Thermal Infrared Remote Sensing. *Innov. Geosci.* **2024**, *2*, 100104. [CrossRef]
18. Sánchez, J.M.; Galve, J.M.; González-Piqueras, J.; López-Urrea, R.; Niclòs, R.; Calera, A. Monitoring 10-m LST from the Combination MODIS/Sentinel-2, Validation in a High Contrast Semi-Arid Agroecosystem. *Remote Sens.* **2020**, *12*, 1453. [CrossRef]
19. Sanchez, J.M.; Galve, J.M.; Nieto, H.; Guzinski, R. Assessment of High-Resolution LST Derived from the Synergy of Sentinel-2 and Sentinel-3 in Agricultural Areas. *IEEE J. Sel. Top. Appl. Earth Obs. Remote Sens.* **2024**, *17*, 916–928. [CrossRef]
20. Guzinski, R.; Nieto, H.; Ramo Sánchez, R.; Sánchez, J.M.; Jomaa, I.; Zitouna-Chebbi, R.; Roupsard, O.; López-Urrea, R. Improving Field-Scale Crop Actual Evapotranspiration Monitoring with Sentinel-3, Sentinel-2, and Landsat Data Fusion. *Int. J. Appl. Earth Obs. Geoinf.* **2023**, *125*, 103587. [CrossRef]
21. Zhou, J.; Liu, S.; Li, M.; Zhan, W.; Xu, Z.; Xu, T. Quantification of the Scale Effect in Downscaling Remotely Sensed Land Surface Temperature. *Remote Sens.* **2016**, *8*, 975. [CrossRef]
22. Mhawej, M.; Abunnasr, Y. Daily Ten-ST-GEE: An Open Access and Fully Automated 10-m LST Downscaling System. *Comput. Geosci.* **2022**, *168*, 105220. [CrossRef]
23. Onačillová, K.; Gallay, M.; Paluba, D.; Péliová, A.; Tokarčík, O.; Laubertová, D. Combining Landsat 8 and Sentinel-2 Data in Google Earth Engine to Derive Higher Resolution Land Surface Temperature Maps in Urban Environment. *Remote Sens.* **2022**, *14*, 4076. [CrossRef]
24. Gorelick, N.; Hancher, M.; Dixon, M.; Ilyushchenko, S.; Thau, D.; Moore, R. Google Earth Engine: Planetary-Scale Geospatial Analysis for Everyone. *Remote Sens. Environ.* **2017**, *202*, 18–27. [CrossRef]
25. Good, E.J.; Ghent, D.J.; Bulgin, C.E.; Remedios, J.J. A Spatiotemporal Analysis of the Relationship between Near-Surface Air Temperature and Satellite Land Surface Temperatures Using 17 Years of Data from the ATSR Series. *J. Geophys. Res. Atmos.* **2017**, *122*, 9185–9210. [CrossRef]
26. Rouse, J.W. *Monitoring the Vernal Advancement and Retrogradation of Natural Vegetation*; NASA: Washington, DC, USA, 1973.
27. Townshend, J.R.G.; Justice, C.O. Analysis of the Dynamics of African Vegetation Using the Normalized Difference Vegetation Index. *Int. J. Remote Sens.* **1986**, *7*, 1435–1445. [CrossRef]
28. Zha, Y.; Gao, J.; Ni, S. Use of Normalized Difference Built-up Index in Automatically Mapping Urban Areas from TM Imagery. *Int. J. Remote Sens.* **2003**, *24*, 583–594. [CrossRef]
29. Jimenez-Munoz, J.C.; Cristobal, J.; Sobrino, J.A.; Sòria, G.; Ninyerola, M.; Pons, X. Revision of the Single-Channel Algorithm for Land Surface Temperature Retrieval from Landsat Thermal-Infrared Data. *IEEE Trans. Geosci. Remote Sens.* **2009**, *47*, 339–349. [CrossRef]
30. Coll, C.; Caselles, V.; Valor, E.; Niclòs, R. Comparison between Different Sources of Atmospheric Profiles for Land Surface Temperature Retrieval from Single Channel Thermal Infrared Data. *Remote Sens. Environ.* **2012**, *117*, 199–210. [CrossRef]
31. Niclòs, R.; Pérez-Planells, L.; Coll, C.; Valiente, J.A.; Valor, E. Evaluation of the S-NPP VIIRS Land Surface Temperature Product Using Ground Data Acquired by an Autonomous System at a Rice Paddy. *ISPRS J. Photogramm. Remote Sens.* **2018**, *135*, 1–12. [CrossRef]
32. Niclòs, R.; Puchades, J.; Coll, C.; Barberà, M.J.; Pérez-Planells, L.; Valiente, J.A.; Sánchez, J.M. Evaluation of Landsat-8 TIRS Data Recalibrations and Land Surface Temperature Split-Window Algorithms over a Homogeneous Crop Area with Different Phenological Land Covers. *ISPRS J. Photogramm. Remote Sens.* **2021**, *174*, 237–253. [CrossRef]
33. Theocharous, E.; Fox, N.P.; Barker-Snook, I.; Niclòs, R.; Garcia Santos, V.; Minnett, P.J.; Göttsche, F.M.; Poutier, L.; Morgan, N.; Nightingale, T.; et al. The 2016 CEOS Infrared Radiometer Comparison: Part II: Laboratory Comparison of Radiation Thermometers. *J. Atmos. Ocean. Technol.* **2019**, *36*, 1079–1092. [CrossRef]

34. Coll, C.; Niclòs, R.; Puchades, J.; García-Santos, V.; Galve, J.M.; Pérez-Planells, L.; Valor, E.; Theocharous, E. Laboratory Calibration and Field Measurement of Land Surface Temperature and Emissivity Using Thermal Infrared Multiband Radiometers. *Int. J. Appl. Earth Obs. Geoinf.* **2019**, *78*, 227–239. [CrossRef]
35. Gillespie, A.; Rokugawa, S.; Matsunaga, T.; Steven Cothern, J.; Hook, S.; Kahle, A.B. A Temperature and Emissivity Separation Algorithm for Advanced Spaceborne Thermal Emission and Reflection Radiometer (ASTER) Images. *IEEE Trans. Geosci. Remote Sens.* **1998**, *36*, 1113–1126. [CrossRef]
36. Rubio, E.; Caselles, V.; Coll, C.; Valour, E.; Sospedra, F. Thermal–Infrared Emissivities of Natural Surfaces: Improvements on the Experimental Set-up and New Measurements. *Int. J. Remote Sens.* **2003**, *24*, 5379–5390. [CrossRef]
37. Garcia-Santos, V.; Valor, E.; Caselles, V.; Mira, M.; Galve, J.M.; Coll, C. Evaluation of Different Methods to Retrieve the Hemispherical Downwelling Irradiance in the Thermal Infrared Region for Field Measurements. *IEEE Trans. Geosci. Remote Sens.* **2013**, *51*, 2155–2165. [CrossRef]
38. Moreno, J.; Alonso, L.; Fernàndez, G.; Fortea, J.; Gandía, S.; Guanter, L.; García, J.; Martí, J.; Melia, J.; De Coca, F.; et al. The SPECTRA Barrax Campaign (SPARC): Overview and First Results from CHRIS Data. *Eur. Space Agency (Spec. Publ.) ESA SP* **2004**, *578*, 30–39.
39. Sobrino, J.A.; Jiménez-Muñoz, J.C.; Sòria, G.; Gómez, M.; Ortiz, A.B.; Romaguera, M.; Zaragoza, M.; Julien, Y.; Cuenca, J.; Atitar, M.; et al. Thermal Remote Sensing in the Framework of the SEN2FLEX Project: Field Measurements, Airborne Data and Applications. *Int. J. Remote Sens.* **2008**, *29*, 4961–4991. [CrossRef]
40. Galve, J.M.; Sánchez, J.M.; García-Santos, V.; González-Piqueras, J.; Calera, A.; Villodre, J. Assessment of Land Surface Temperature Estimates from Landsat 8-TIRS in A High-Contrast Semiarid Agroecosystem. Algorithms Intercomparison. *Remote Sens.* **2022**, *14*, 1843. [CrossRef]
41. Fox, N. *Fiducial Reference Measurements for Validation of Surface Temperature from Satellites (FRM4STS) D-180 FRM4STS Final Report*; NPL: New Delhi, India, 2019.
42. Pu, R.; Bonafoni, S. Reducing Scaling Effect on Downscaled Land Surface Temperature Maps in Heterogenous Urban Environments. *Remote Sens.* **2021**, *13*, 5044. [CrossRef]
43. Bisquert, M.; Sánchez, J.M.; Caselles, V. Evaluation of Disaggregation Methods for Downscaling MODIS Land Surface Temperature to Landsat Spatial Resolution in Barrax Test Site. *IEEE J. Sel. Top. Appl. Earth Obs. Remote Sens.* **2016**, *9*, 1430–1438. [CrossRef]
44. Puchades-Yago, J.; Calera-Belmonte, A.; Galve, J.M.; Sánchez-Tomás, J.M.; González-Piquera, J. Calibración Cruzada Entre Landsat-8 y Sentinel-2 Para Configurar Una Constelación Multisensor. In Proceedings of the Teledetección para una Agricultura Sostenible en la era del Big Data.Actas del XIX Congreso de la Asociación Española de Teledetección, Pamplona, Spain, 29 June–1 July 2022; Available online: http://www.aet.org.es/?q=congresos:Pamplona (accessed on 9 July 2025).
45. Nash, J.E.; Sutcliffe, J.V. River Flow Forecasting through Conceptual Models Part I—A Discussion of Principles. *J. Hydrol.* **1970**, *10*, 282–290. [CrossRef]
46. Coll, C.; Galve, J.M.; Sánchez, J.M.; Caselles, V. Validation of Landsat-7/ETM+ Thermal-Band Calibration and Atmospheric Correction with Ground-Based Measurements. *IEEE Trans. Geosci. Remote Sens.* **2010**, *48*, 547–555. [CrossRef]
47. Niclòs, R.; Perelló, M.; Puchades, J.; Coll, C.; Valor, E. Evaluating Landsat-9 TIRS-2 Calibrations and Land Surface Temperature Retrievals against Ground Measurements Using Multi-Instrument Spatial and Temporal Sampling along Transects. *Int. J. Appl. Earth Obs. Geoinf.* **2023**, *125*, 103576. [CrossRef]
48. Galve, J.M.; Sánchez, J.M.; Coll, C.; Villodre, J. A New Single-Band Pixel-by-Pixel Atmospheric Correction Method to Improve the Accuracy in Remote Sensing Estimates of LST. Application to Landsat 7-ETM+. *Remote Sens.* **2018**, *10*, 826. [CrossRef]
49. García-Santos, V.; Coll, C.; Valor, E.; Niclòs, R.; Caselles, V. Analyzing the Anisotropy of Thermal Infrared Emissivity over Arid Regions Using a New MODIS Land Surface Temperature and Emissivity Product (MOD21). *Remote Sens. Environ.* **2015**, *169*, 212–221. [CrossRef]
50. García-Santos, V.; Valor, E.; Caselles, V.; Coll, C.; Burgos, M.Á. Effect of Soil Moisture on the Angular Variation of Thermal Infrared Emissivity of Inorganic Soils. *IEEE Geosci. Remote Sens. Lett.* **2014**, *11*, 1091–1095. [CrossRef]